EnerKíte

AIRBORNE WIND ENERGY CONFERENCE 2017

Comparison of Launching and Landing Approaches

Burkhard Rieck, Maximilian Ranneberg, Ashwin Candade, Alexander Bormann (EnerKíte GmbH); Stefan Skutnik (TU Berlin)

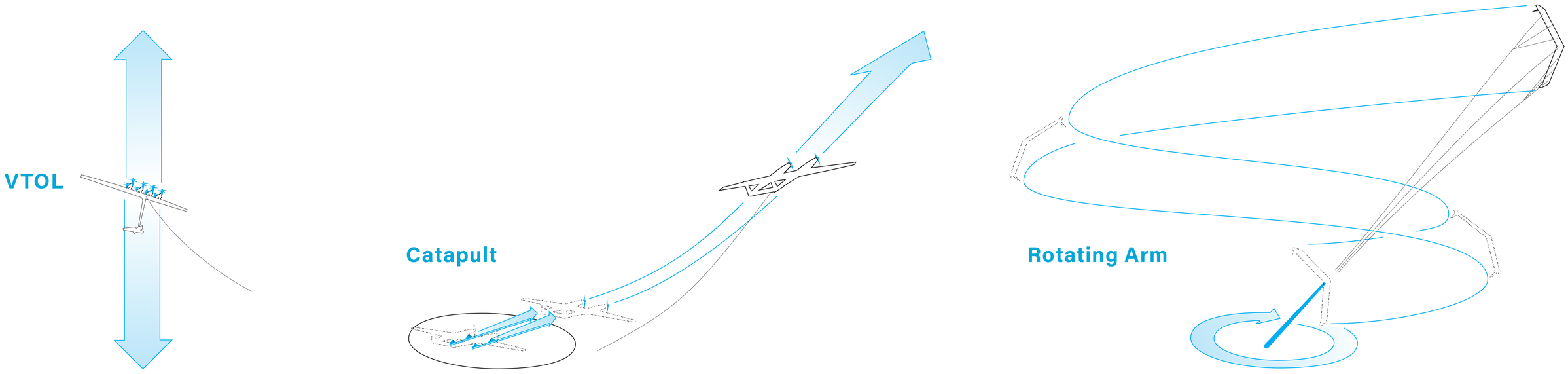

Fig. 1: Principles of the compared take-off and landing systems. The calculations below use the same EK200 wing, the drawings show wings used in the AWE community for the respective system.

Comparison of Systems

A comparison of the three launching and landing systems for a 100kW AWES with nominal power output at 8 m/s at 200 m is presented on the basis of the defined requirements, airborne systems, additional wing area, additional mass, power and maturity of technology.

	Requirements						Systems		Wing Area	Mass		Power		Maturity
	1	2	3	4	5	6	On-Ground	Airborne		On-Ground	Airborne	On-Ground	Airborne	
Rotating Arm							+++		0%	+++	0%	20%	0%	
Catapult & Thrust							++	+	7.5%	++	5%	5%	9.3%	
VTOL							+	+++	17%		29%	0%	74%	

Legend: Good | Average | Poor

Tab. 1: Comparison of take-off and landing systems. The numbers were derived from the scenarios outlined below. Percentages w.r.t. no launch & landing system mass and nominal power.

Introduction

For the commercial success of Airborne Wind Energy, it is imperative to have a scalable and cost efficient system that is capable of reliable launching and landing. For the rigid wing technology present at EnerKíte, three suitable landing and launching techniques, namely vertical take-off, catapult, and rotating arm are compared in this analysis.

Details of the simulation of the rotational landing and launching system, followed by comparisons with field trials are then presented.

To facilitate comparisons, a set of major requirements for landing and launching of the EnerKíte wing is outlined.

Requirements

1 Defined docked state. For secure storage of the wing in normal and extreme weather.
2 High capacity factor designs. Suitable for low-mass, high-area systems.
3 Wind conditions. Ability to cope with rapid change in wind direction, gusts and turbulence.
4 Behaviour in case of airborne system failure.
5 Behaviour in case of on-ground system failure.
6 Scalability. Development of cost and complexity with increasing wing size.

The different masses and powers (airborne and on-ground) are estimated for the three techniques, revealing the scaling effects with respect to different power ratings, wing sizes, weights and other concerns stemming from economic, safety and certification aspects. From the comparison, the choice at EnerKíte for a rotational landing and launching system is motivated.

The evaluation from poor to good and are based on process complexity, necessity of additional systems, derived dependence on power and weight, cost and feasibility.

For example, the VTOL concept is poor with respect to high capacity factor designs, because large wings lead to high installed airborne power, regardless of the nominal design wind speed.

Mass

Effect on Power Curve

To analyse the effect of different wing masses on the system, the power curve and yield calculation method described in [1] is used to find optimised systems with the same nominal power output at 8 m/s wind speed at 200 m altitude and thus similar power curves and yield. A design with 2.5 kg/m² defines the target for EK and the systems are compared to this case without a launch and landing system.

The effect of mass becomes less important at higher wind speeds, thus high mass-to-area ratio systems are more suitable for high nominal wind-speed designs. Above 10 kg/m² the power curve calculations become difficult at low wind speeds, as the inertia force during sharp turns cannot be overcome by the aerodynamic force at these wind speeds.

Mass/Area	[kg/m²]	2.5	3.5	4.5	5.5	6.5	7.5	8.5	9.5
Area	[m²]	33.4	34.3	34.7	36.0	37.6	39.3	41.4	42.4
Nominal Tether Force	[kN]	45.7	45.7	45.5	46.8	48.6	50.8	52.9	54.9
Start Wind Speed	[m/s]	2.4	2.4	2.5	2.8	3.0	3.2	3.3	3.4

Systems

The current champion of ultra-light motors has been developed by Siemens [2] and arrives at 5 kW/kg, although that is just the motor without electronics, electrics or housing. In [3] the best available Li-Ion Technology is assessed to arrive at 200 Wh/kg and, somewhat more prohibitive, not more than 2 kW/kg maximum power output. Both components need additional hardware, but we neglect them for a best-case scenario here.

Vertical Take-Off

This concept uses thrust from additional rotors to lift and manoeuvre the wing during take-off and landing. Here, we use the same formulas that were used in [4]. However, the system is additionally iterated to arrive at similar power curves as described above. To incorporate this effect, the start wind speed is fitted using a square root function (as the airspeed is roughly linear with the wind-speed and the force depends on the airspeed squared), while force and area are linear functions. Assuming a specific weight of a strengthened system-free wing of 5 kg/m² to accomodate the additional loads and masses the values in the table were derived.

For the necessary power, 150% of the hover power was assumed as well as a rotor area of 10% of the total wing. Note that this, as well as the mass assumptions in general, is optimistic.

An only marginally strengthened wing with a specific mass of 3 kg/m² would lead to an additional airborne power of 28% of the nominal power, an additional 20% airborne mass, with a 5% increase in wing area. Note that AWE wings are capable of extremely high loads at very low weights. Thus, the forces occurring during take-off and landing can be, during gusts, several multiples of the wing weight.

Catapult

For the catapult launch, the common energy approach was utilised to determine the power required on-ground by the catapult for the launch phase similar to [4]. During this phase, it was assumed that the catapult power is augmented by the airborne thrust as well. Furthermore, to account for changing wind directions, the launch system should be able to orient it self, leading to an additional 8% of the required on-ground power. Following the ground launch, the power required by the airborne rotors to reach an altitude of 100 m was calculated using actuator disk theory and elementary flight mechanics [5]. The system was iterated in order to converge on the additional mass of the on board propulsion system for a base specific weight of 4 kg/m². Similar to the vertical take-off variant, 150% of the required thrust was assumed, with a 10% zero-mass rotor to wing area ratio.

For an only marginally strengthened wing with a specific mass of 3 kg/m², the airborne power increases to 6.5% of the nominal power, with a 3.5% increase in wing area.

Rotating Arm

In a steady-state zero-mass kite system with aerodynamic coefficients C_L, C_D , due to the law of sines, the fact that $C_L / C_D = \tan\tau$ and the geometry it holds that

$$R\left(\frac{C_L}{C_D}\sin\phi - \cos\phi\right) = L$$

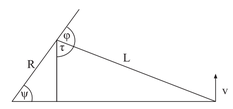

That is, the tether length at which we can rotate without any wind is roughly $R\frac{C_L}{C_D}$ or 120 m for a system Lift-over-Drag of 10 and an arm length of 12 m. Steep elevation angles θ reduce that length by roughly $\cos^2\theta$. From the above formula, together with the assumption of using 10% of the nominal force during rotation, power and torque can be derived. This leads to a necessary power of 20% of the nominal power. Note that these results change with the mass of the kite.

While EK wings are lightweight and the mass is negligible compared to the tether force at 10% nominal force, this changes for very heavy wings.

Point Mass Model

Model

The arm is modelled by a motor turning the arm with a kinetic energy of $\frac{1}{2}J_a\omega_a^2$ and work: $\int M_a d\phi_a$. The position of the arm end is given by $\hat{r}_a(\phi_a) = R_a[\cos(\phi_a), \sin(\phi_a), 0]^T$. The winch model is similar to the arm model, with J_w, M_w, ω_w and $L = R_w\phi_w$.

The rod analogy leads to the Lagrange constraints (1) where the Right-Hand-Side is defined by the actuator controls. The kite is a point-mass with aerodynamic force $F(v_a)$. The kite is controlled with a roll angle, which moves the lift axis along the orthogonal plane of the airspeed. Deriving the Lagrangian using above model assumptions leads to the differential-algebraic equations (1-5).

$$(x - r_a(\phi_a))^T (x - r_a(\phi_a)) = \phi_w^2 R_w^2 \quad (1)$$

$$m\ddot{x} - \lambda(x - r_a) = F \quad (2)$$

$$J_w\dot{\omega}_w + \lambda R_w^2 \phi_w = M_w \quad (3)$$

$$J_a\dot{\omega}_a - \lambda(x - r_a)^T(\partial_{\phi_a} r_a) = M_a \quad (4)$$

$$J_a\dot{\omega}_t - \lambda(x - r_a)^T(\partial_{\phi_t} r_a) = M_t \quad (5)$$

Optimal Control

While it is not surprising that during no-wind conditions rotations with increasing and decreasing tether lengths are possible, necessary controls and trajectories at higher wind speeds are less obvious. The figure shows the periodic trajectories of several optimal control problems. Each trajectory follows closely the same angle between arm and kite, applies a constant torque on the arm and uses slow winch torque variations. The wind speed here is 6 m/s. To keep the airspeed nearly constant, the winch is reeled in and out which leads to the asymmetric trajectories. This happens automatically, as for a constant torque the rise and fall of airspeed leads to the acceleration of the tether and winch. While control of a kite in changing wind conditions is by no means an easy task, especially if three lines are used to control angle of attack as well, the problem of doing so during a rotating launch and landing manoeuvre is in principle not significantly more complicated.

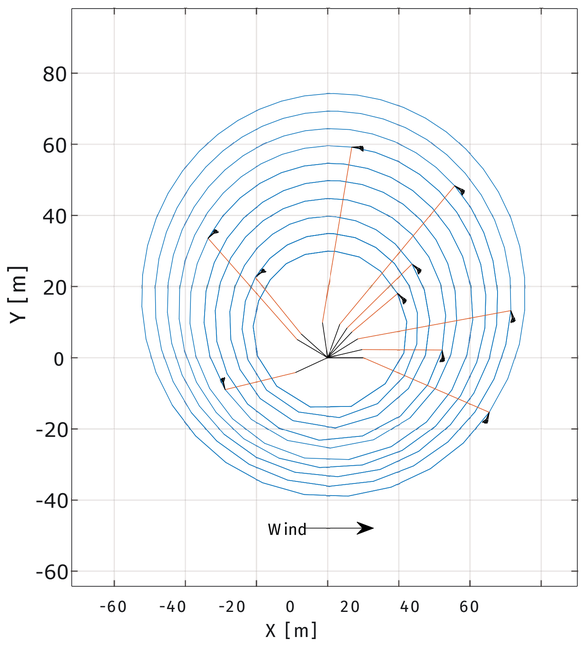

Fig. 2: Family of periodic optimal control trajectories.

Detailed Simulation and Field Trials

The graph below shows the control line difference with respect to the main control line during rotation at short lengths at low wind speeds. These control lines are the ones that are connected to the bridle in the simulation snapshort right. Compared are simulations using a detailed simulation model and data from field tests. The control line difference relates to the angle of attack that needs to be maintained, while the wind direction changes constantly during rotation. Note that these lengths are not commanded, but are the result of this control endeavour and hence this graph shows a good correlation between simulation and actual wing behaviour.

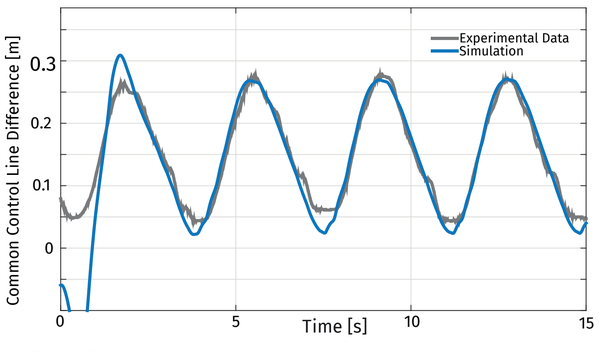

Fig. 3: Comparison of collective control in simulation and in field test.

Fig. 4: Visualization of near-arm trajectory

References

[1] Maximilian Ranneberg et al. "Fast Power Curve and Yield Estimation of Yo-Yo Airborne Wind Energy Systems.". In: Airborne Wind Energy (2018). [2] Siemens Motors for eAircraft. url: https://www.siemens.com/press/en/feature/2015/corporate/2015-03-electromotor.php [3] Xing Luo et al. "Overview of current development in electrical energy storage technologies and the application potential in power system operation". In: Applied Energy 137 (2015). [4] Lorenzo Fagiano and Schnez. Stephan. "On the take-off of airborne wind energy systems based on rigid wings.". In: Renewable Energy 107 (2017). [5] Barnes Warnock McCormick. Aerodynamics, Aeronautics, and Flight mechanics. English. 2nd ed. New York: Wiley.